HHS Public Access

Author manuscript

J Orthop Res. Author manuscript; available in PMC 2023 November 01.

Published in final edited form as:

J Orthop Res. 2022 November ; 40(11): 2609–2619. doi:10.1002/jor.25295.

Objective Evaluation of Chondrocyte Density & Cloning after Joint Injury using Convolutional Neural Networks

Linjun Yang[1,2], **James A. Martin**[1,2], **Marc J. Brouillette**[1], **Joseph A. Buckwalter**[1], **Jessica E. Goetz**[1,2]

[1]Department of Orthopedics and Rehabilitation, University of Iowa, Iowa City, IA, 52242, USA

[2]Department of Biomedical Engineering, University of Iowa, Iowa City, IA, 52242, USA

Abstract

Variations in chondrocyte density and organization in cartilage histology sections are associated with OA progression. Rapid, accurate quantification of these two features can facilitate the evaluation of cartilage health and advance the understanding of their significance. The goal of this work was to adapt deep-learning-based methods to detect articular chondrocytes and chondrocyte clones from safranin-O-stained cartilage to evaluate chondrocyte cellularity and organization. The U-net and "you-only-look-once" (YOLO) models were trained and validated for identifying chondrocytes and chondrocyte clones, respectively. Validated models were then used to quantify chondrocyte and clone density in talar cartilage from Yucatan minipigs sacrificed one week, 3 months, 6 months, and 12 months after fixation of an intra-articular fracture of the hock joint. There was excellent/good agreement between expert researchers and the developed models in identifying chondrocytes/clones (U-net: R^2=0.93, y=0.90×–0.69; median F1 score: 0.87 / YOLO: R^2=0.79, y=0.95×; median F1 score: 0.67). Average chondrocyte density increased one week after fracture (from 774 to 856 cells/mm^2), decreased substantially 3 months after fracture (610 cells/mm^2), and slowly increased 6 and 12 months after fracture (638 and 683 cells/mm^2, respectively). Average detected clone density 3, 6, and 12 months after fracture (11, 11, 9 clones/mm^2) was higher than the 4–5 clones/mm^2 detected in normal tissue or one week after fracture and show local increases in clone density that varied across the joint surface with time. The accurate evaluation of cartilage cellularity and organization provided by this deep learning approach will increase objectivity of cartilage injury and regeneration assessments.

Keywords

Articular Cartilage Histology; Chondrocyte; U-net; YOLO; Deep Learning

Corresponding Author: Jessica E. Goetz, Ph.D., Orthopedic Biomechanics Lab, 2181 Westlawn Building, Iowa City, IA 52242-1100, Phone: (319) 384-4275, Fax:(319) 335-7530, jessica-goetz@uiowa.edu.

Author Contributions Statement: L.Y. developed the deep learning models, analyzed the data, and drafted the manuscript text. J.M. M.B., and J.B. helped annotate images for model development and read and edited the manuscript. J.G. supervised the whole work, annotated images for model development, performed the statistical analysis, and read and edited the manuscript.

TECHNOLOGY SHARING STATEMENT

If interested in collaborating regarding the trained models presented here, please contact the investigators directly.

INTRODUCTION

In research settings, histological analysis is a commonly used technique for evaluation of cartilage health, determining severity of osteoarthritis (OA), and evaluating efficacy of therapeutic approaches. It is common practice with this approach to evaluate cartilage cellularity and chondrocyte organization. Chondrocyte density estimated from histologic sections has been accepted as a measure of articular cartilage health. Previous work indicates that optimal chondrocyte density is necessary to maintain cartilage tissue, while declining chondrocyte density is associated with degeneration of articular cartilage in OA and with aging.[1] In contrast, chondrocyte cloning - formation of non-linear clusters of chondrocytes - is considered one of the markers of osteoarthritis,[1] although the significance and events responsible for cloning are not well understood. Semi-quantitative, subjective, categorical evaluations of cartilage cellularity, such as those performed during application of Mankin[1] and OARSI[2] scoring, have limitations including uncertain accuracy and reproducibility.[3] For these reasons, the ability to rapidly quantitate chondrocyte density and cloning could help advance understanding of these phenomena in the pathophysiology of osteoarthritis and in articular cartilage regeneration, repair, and aging.

One previously reported approach uses image analysis algorithms to automatically identify chondrocyte density and red intensity values of pixels within the segmented cartilage and assigns cellularity and PG depletion Mankin sub-scores based on deviation of those quantitative values from pre-defined normative values.[4, 5] While that program achieved good agreement with human experts for the Mankin structural sub-score (linear regression; R^2: 0.87, slope: 0.84) and the PG depletion sub-score (R^2: 0.63, slope: 0.70), there was poor agreement with human experts on the cellularity sub-score (R^2: 0.07, slope: 0.21).[4] This poor agreement may result from the simple thresholding segmentation and edge detection used to identify chondrocytes,[4] two image analysis techniques which are far from being robust to the huge variation in tissue appearance during cartilage degeneration. Erroneous chondrocyte density calculations could artificially elevate the assigned cellularity sub-score by classifying it as either hypercellular or hypocellular.[1] Furthermore, difficulty in accurately segmenting chondrocytes substantially reduces the ability to automatically identify chondrocyte cloning. To accurately quantify cartilage cellularity and/or accurately assign cellularity scores, more sophisticated image analysis algorithms that can accommodate the wide variety of chondrocyte appearances and organization in degenerating cartilage are required.

Conveniently, modern deep-learning-based approaches have been reported to have achieved great success in a variety of computer vision tasks.[6–10] A convolutional neural network (CNN) is one common deep learning method in which the model is trained to analyze a given image type by using pairs of similar input images and the corresponding correct output data (ground truth) – a technique called supervised learning. With this technique, a CNN model is able to learn inter-related hierarchical features from the image, which allows it to accurately classify, detect, and segment objects with variable appearances.[8, 9] CNN-based approaches have previously been applied very successfully in orthopedic research to perform tasks such as grading/classifying radiographic knee images[11, 12] and segmenting bone and soft tissues from MR images.[13–15] CNN-based approaches have also achieved

tremendous success in a variety of digital pathology applications. For example, Bejnordi *et al* have assessed different CNN models for detecting lymph node metastases in women with breast cancer, and achieved a model that outperforms expert pathologists.[16] Similarly, Nagpal *et al* developed and validated a CNN model to stage prostate cancer, which resulted in higher accuracy than a group of pathologists.[17] There are also CNN-based studies ranging from detecting sub-cellular (nuclei) components[18, 19] to segmentations of glandular structures[20, 21] in histology images.

However, applications to cartilage analysis have been more limited. Recent work by Powel *et al*[22] describes using a CNN-based image classifier to automatically assign a Bern score to evaluate chondrogenicity of engineered cartilage,[23] and Rytky *et al* has developed a CNN model to automatically segment calcified cartilage to study its modification during OA progression.[24] Based on this previous success, our goal in this work was to develop and implement methods to accurately map chondrocyte density and chondrocyte cloning across the entire articular cartilage surface using a combination of CNN models and spatial information. We aimed to adapt our previously trained U-net model[25] and a "you only look once" (YOLO)[8] model to segment individual chondrocytes and identify chondrocyte clones in cartilage. We hypothesized that fully automated chondrocyte density and clone detection achieved with CNN models would have excellent agreement with gold-standard human expert cell/clone identification. Further, we hypothesized that application of the trained models would be able to identify subtle progressive changes in chondrocyte cellularity and organization associated with development of post-traumatic osteoarthritis after a joint injury.

METHODS

CNN Models – U-net and "you only look once" (YOLO)

To accurately identify individual chondrocytes through the full depth of articular cartilage, we retrained our previously reported U-net model from scratch.[25] The previous model had been developed by adding one batch normalization layer[26] between each convolutional layer and its following ReLU activation function[27] in the original U-net architecture.[9] Zero-padding was used for all the convolutional layers, allowing the output segmentation image to share the same size as the input image. The sigmoid activation function[27] was used after the last convolutional layer to output values between 0 and 1 at each pixel. Under this adaption, the model takes the input image of size 512 × 512 × 3 (pixel x pixel x RGB) and outputs a single channel probability image (512 × 512), with each output pixel representing the probability of it being a chondrocyte. Pixels with predicted probability values higher than 0.5 were labeled as cell pixels. To emphasize segmentation accuracy for smaller and more closely packed cells, such as would be found in the superficial zone or in a clone, additional images of superficial zone cartilage were included in the training set. The previous U-net model[25] was then retrained to optimize a modified binary cross entropy loss function that was weighted to emphasize smaller superficial zone chondrocytes and chondrocytes that were closely adjacent (Figure 1).

To identify chondrocyte clones, the YOLO object detection model[8] was used. YOLO predicts a set of bounding boxes to localize objects, with a label for each box representing the "class" of the detected object. To build our YOLO model, the contracting path of our

retrained U-net was copied, which allowed the YOLO model to utilize previously learned chondrocyte features (a method termed transfer learning). Additional convolutional layers and max pooling layers were stacked after the copied path to allow the YOLO model to learn local image context for the existence of a clone. To detect multiple clones that can appear within a single image, our YOLO model was implemented to predict one bounding box in each cell of an 8×8 grid defined over the 512×512 pixel input image (Figure 2). The bounding box information predicted in each grid cell included bounding box size, centroid coordinates, and a probability value (between 0 and 1) of detecting a clone centered within the grid cell (Figure 2). Bounding boxes with a probability value >0.5 were considered clones. Training the YOLO was achieved by optimizing a previously described loss function[8] which forces clone detection with high-probability, closely fitting bounding boxes.

The U-net and YOLO models were trained using previously generated Safranin-O and fast green-stained histological sections of rabbit articular cartilage with varying degrees of arthritic changes induced by ACL transection[28] and medial meniscus destabilization.[29] Sections were digitized using a stage scanner microscope (Olympus VS110, Olympus America Inc., Center Valley, PA, USA) at a resolution of 322.25 nm per pixel. 512 × 512-pixel images encompassing chondrocytes/clones of varying size, shape, appearance, and zonal origin were cropped from the digitized histology sections. 325 training images, consisting of our previous 235 training images[25] and additional 90 images of superficial zone cartilage, and a separate set of 24 validation images were used for retraining the U-net. A different set of 300 training images and 25 validation images was used for training the YOLO model.

Training images were cropped using ImageJ (NIH, https://imagej.nih.gov/ij/) software. All training and validation images for the U-net were manually segmented using MATLAB R2020a (The MathWorks, Natick, MA) by a single individual with >3 years' experience identifying chondrocytes in histological sections of cartilage. Clones in the training images were annotated (enclosed in a bounding box) in MATLAB by the same individual, with a clone defined as a cluster that includes at least three different chondrocytes encapsulated by the same lacuna. Cloning validation images were developed from the consensus annotation by three expert cartilage researchers. To replicate in-practice variability of histology images, data augmentation including image rotation, mirroring, and brightness adjustment was applied to the training images for both models using the Python scikit-image library.[30]

The U-net and YOLO were implemented using the open-source deep learning framework Keras (https://keras.io/) with the TensorFlow backend. We would be available to share elements of our codes to the interested researchers. Models were trained using an NVIDIA Tesla K80 GPU. The U-net was trained for 100 epochs (requiring 120 minutes), while the YOLO was trained using 120 epochs (requiring 150 minutes). Inference time to analyze a 512 × 512 image was 0.1 s and 0.12 s for the U-net and YOLO, respectively. An F1 score,[21] which evaluates the ratio of true positive cell detections among all cell detections by the model, was calculated for each validation image at each epoch. The final U-net and YOLO models were selected based on achieving the highest average F1 score on the validation images in each training set. A secondary validation of the selected U-net

and YOLO models was then conducted using 30 different expert-annotated testing images unseen by the algorithm during training. Agreement between the trained CNN models and experts was evaluated using F1 scores and linear regression to evaluate chondrocyte and clone identification and intersection over union (IOU) to evaluate accuracy of chondrocyte segmentation. These non-normally distributed data (Shapiro-Wilk test; Prism 9, GraphPad Software LLC, San Diego, CA) are reported as medians with 95% confidence intervals (CIs).

Cellularity Changes after Joint Injury

The validated CNN models were then applied to existing sets of histological sections of articular cartilage in order to document the natural history of changes in chondrocyte density and organization after an intra-articular fracture (IAF) in a Yucatan minipig PTOA model.[31] In this model, impact-induced IAFs in the hock joint (ankle analog) of skeletally mature minipigs (average 24 months of age at fracture) are surgically fixed using open reduction internal fixation (ORIF). From previous[31, 32] and ongoing studies, 5 μm-thick Safranin-O/fast green/Wiegert's hematoxylin-stained sagittal histological sections of the medial talus were available from animals sacrificed one week, 3 months, 6 months, and 12 months after fracture fixation. Histological tissue sections from joints of breed and age-matched healthy, unfractured pigs were also available. All sections had been prepared according to the same histological processing protocol[2] and digitized as described above.

A continuous, 15-mm cartilage span centered within the weightbearing area was selected for analysis and segmented using a previously developed semi-automated segmentation algorithm[4] (Figure 3). A sliding-window approach was then used to automatically divide the entire 15-mm cartilage span into 512 × 512-pixel image tiles (Figure 3-B), each of which was analyzed using the validated U-Net and YOLO models to segment individual chondrocytes and detect chondrocyte clones, respectively. Given that a chondrocyte or a clone may be split into adjacent image tiles by sliding-window locations and hence missed by the U-Net or YOLO, the process was repeated on additional image tiles of the same size acquired after shifting the sliding window by an offset of half the window size in the horizontal and then again in the vertical direction (Figure 3-B). Cell segmentations and clone bounding boxes in each image tile were projected back to the associated window location within the full cartilage geometry (Figure 3-C). Chondrocyte segmentations from all the regular tiles were projected first, then segmentations from the center span of the horizontally offset tiles were added, and finally segmentations from the center span of the vertically offset tiles were added. This method preserved the more accurate cell segmentations from the center of each tile and covered the seams between regular tiles (Figure 3-B). In contrast, all chondrocyte clone bounding boxes from both the regular and additional tiles were projected back to the cartilage segmentation, and subjected to non-maximal suppression[33] to remove any redundant, less accurate bounding boxes.

Three different metrics were calculated to evaluate cartilage cellularity: chondrocyte density, clone density, and percentage of chondrocytes that reside in a clone. To calculate densities, the number of chondrocytes or clones whose centroid was within the segmented cartilage were divided by the cartilage area. Clone chondrocytes were defined as those whose

centroids were located within the bounding box of a clone (Figure 3-C). The number of clone chondrocytes was divided by the total number of chondrocytes identified in the cartilage. These three metrics were calculated for the entire joint, as well as mapped in 1.5 mm increments across the weightbearing cartilage. The 30–40% positions articulated with the healing fracture line. These data were normally distributed (Shapiro-Wilk test); and therefore, one-way ANOVA with post-hoc Tukey's tests was used to compare cellularity values between post-operative timepoints (normal, one week, 3 months, 6 months, and 12 months; n = 5 for all). Repeated measures two-way ANOVA with post-hoc Tukey's tests was used to evaluate differences between joint locations and post-operative timepoints (GraphPad Prism 9).

RESULTS

The optimal U-net was selected at the 82nd epoch with a median F1 score of 0.89 (95% CI: 0.88 to 0.93) on the training validation images, and the optimal YOLO was selected at the 105th epoch with a median F1 score of 0.80 (95% CI: 0.67 to 1.00) on the training validation images. Those F1 score values indicated good detection accuracy (good = 0.70–0.90)[21] by each model. In the secondary validation, the U-net achieved an excellent agreement with the average counts by the experts (Figure 4; $R^2 = 0.93$, $y = 0.90\times - 0.69$) and a close-to-excellent median F1 score (median: 0.87; 95% CI: 0.84 to 0.89). The average IOU between the U-net segmentation and manual segmentation of each chondrocyte was 0.849, indicating high accuracy of U-net chondrocyte segmentations.[34] The three expert researchers' agreement identifying clones was good (ICC = 0.76).[35] Despite relatively a lower median F1 score (median: 0.67; 95% CI: 0.57 to 0.89) for clone detection, the YOLO still achieved good agreement with the average counts by the experts (Figure 4; $R^2 = 0.79$, $y = 0.95\times$). Both models were found to be able to identify chondrocytes/clones of variable size, shape, and appearance (Figure 4).

Differences in cellularity were found between the normal and the different post-operative timepoints (Table 1). Average chondrocyte density one week after fracture (mean: 856 cells/mm^2; 95% CI: 748–963 cells/mm^2) was slightly higher than normal chondrocyte density (mean: 774 cells/mm^2; 95% CI: 742–806 cells/mm^2; p=0.573) and significantly higher than at 3 months (mean: 610 cells/mm^2; 95% CI: 491–729 cells/mm^2; p=0.006), 6 months (mean: 638 cells/mm^2; 95% CI: 470–806 cells/mm^2; p=0.016), and 12 months (mean: 683 cells/mm^2; 95% CI: 556–810 cells/mm^2; p=0.077) after fracture (Figure 5-A). Clone density and percentage of chondrocytes in clones 3, 6, and 12 months after fracture was higher than in normal cartilage or at one week postoperatively, however these differences did not reach statistical significance (Figure 5-B, C; p>0.1 for all pair-wise comparisons).

Local cellularity differences were noted among the different post-injury timepoints. At the anterior positions, chondrocyte densities were lower 3, 6, and 12 months after fracture than after one week or in normal tissue. Cell density was the lowest 3 months after fracture and was significantly lower than densities in normal tissue or one week after fracture at the 10% (p=0.032/0.012), 20% (p=0.107/0.024), and 30% (p=0.006/0.039) positions (Figure 6-A). One week after fracture, chondrocyte densities in the posterior locations were higher than in normal tissue and significantly higher than at 3, 6 and 12 months: 60% (p=0.137, 0.049,

0.649 for 3, 6, 12 months, respectively), 70% (p=0.164, 0.096, 0.556), 80% (p=0.108, 0.010, 0.428), 90% (p=0.023, <0.0001, 0.046), and 100% (p=0.002, < 0.0001, 0.067). Chondrocyte densities 3, 6, and 12 months after fracture were also lower than the normal group at the posterior positions, although these differences did not reach statistical significance.

Locally, significantly higher clone density/percentage of chondrocytes in clones was found 3, 6, and 12 months after fracture (Figure 6-B, C; Table 2). Local clone density at 3 months was significantly higher than the normal group at the 70% position (p=0.013) which is moving into weightbearing tissue that was not directly affected by the fracture. By 6 and 12 months after fracture, significantly higher clone densities than in the normal and/or one-week groups were found more peripherally in the joint (the 20% and 80% positions). Clone density at 6 months was significantly higher than in normal or one week at the 20% position (p=0.026, 0.021) and at 12 months clone density was higher than in the normal (p=0.057) and one-week (p=0.047) groups at the 80% position. Variations in the percentage of chondrocytes in a clone were very similar to the local variations of clone density (Figure 6-C).

DISCUSSION

Histological analysis remains among the most commonly used research techniques to evaluate the health of cartilage. In this work, we trained, validated, and implemented two different CNN models to quantify the progressive chondrocyte cellularity changes after joint/cartilage injury. The trained U-net and YOLO models developed for this purpose were validated to be accurate for identifying chondrocytes and clones by achieving good agreement with manual assessment by expert researchers. These algorithms proved to be extensible for use identifying chondrocytes and chondrocyte clones in degenerating minipig cartilage, and they were able to identify progressive cellularity changes with time after joint injury.

While there are several CNN models that could be suitable for chondrocyte identification,[7, 10] the U-net was selected for chondrocyte detection because it has demonstrated state-of-art performance on a similar cell detection task,[9] and it provides boundary information from chondrocyte segmentation that can be useful for future studies related to co-localization of functional cellular stains and specific morphological structures. In contrast, as relatively little is known about the importance of the morphology of clones, a simple bounding-box-based detection method was used for clone detection in this work. The YOLO was selected over other bounding-box-based methods for its developmental and implementation simplicity. Specifically, it is a single CNN model that can be developed and trained end-to-end to predict bounding box probability and coordinates simultaneously.[8] Similar methods have two stages, requiring independent development of a bounding box generator and an image classifier,[7, 36] which can be more laborious and slower. If clone morphology, rather than simple detection, becomes more important in future work, adapting the U-net trained to segment chondrocytes using transfer learning would likely be successful for that purpose.

The U-net model reported here is a retrained version of our previously reported model which had been selected based on providing the lowest average loss value during training.[25] However, that model, chosen to minimize weighted loss at each pixel, did not correspond to the highest detection accuracy at the cell level. Therefore, in addition to modifications made to emphasize detection of small, closely packed chondrocytes, the retrained model was selected based on providing the highest F1 score, which reflected the best cell detection accuracy as compared with the gold-standard manual segmentations. To maximize functional accuracy, a similar process was followed during the training of the YOLO. This approach of selecting a model based on performance was used to avoid choosing an overfit model, while the secondary validation of the selected model (on different testing images) was intended to assess generalizability to unseen image data.

Estimated chondrocyte densities in pig cartilage were close in magnitude to previously reported values in a large animal (~1000 cells/mm^2).[37] Reduced chondrocyte density and more active cloning was found beginning 3 months after intra-articular fracture, which corroborates the elevated histological scoring of PTOA previously reported in this animal model at the same time point.[31] Chondrocyte density began to progressively, though not significantly, rebound by 6 months (increased 28 cells/mm^2; p=0.716) and 12 months (increased 73 cells/mm^2; p=0.5734) after the fracture. Despite greater clone densities at 6 and 12 months, the progressive increases in chondrocyte density were found to be mainly from increases in chondrocytes not associated with clones (non-clone related chondrocyte density: 580, 596, 642 cells/mm^2 for 3, 6, and 12 months after fracture, respectively). At 6 and 12 month postoperative timepoints, the combination of lower than normal chondrocyte density, increased number of chondrocyte clones, and increasing chondrocyte cellularity outside clones indicate progressive arthritic changes, but not necessarily a linear progression through the stages of cellularity outlined in the Mankin scoring system.[1] Local increases in clone density at 3 months were found close to the region that articulates with the healing fracture line, and then more anteriorly and posteriorly relative to that location by 6 months and 12 months after fracture. These findings would indicate spatial progression of cartilage abnormalities through the joint that are associated with time after injury, however determining the mechanism responsible for this would require a separate study.

There are several limitations in this work that need to be considered. The first is that we have trained the YOLO model to identify a chondrocyte clone based on our empirical definition of >3 non-linearly organized chondrocytes in a single lacuna. These criteria were chosen to provide a standardized morphological description of the appearance of a specific feature of osteoarthritic cartilage identified in the Mankin scoring scheme as “cloning”.[1] This term “clone” has been used interchangeably with the term “cluster” or “proliferation” in other scoring schemes.[2] A true clone would imply that all the chondrocytes present in any given instance of this feature were derived from a single cell, and such an assessment would require a detailed analysis of cell proliferation markers that is not feasible in Safranin-O sections. While determining the true clonal/proliferative nature of the cells in these features is outside the scope of this work, a future study combining this automated feature detection approach with specific stages of chondrocyte proliferation/activity could provide important information about the time course of chondrocyte function throughout the course of osteoarthritic cartilage degeneration after joint injury. It would also be interesting to relate

such findings to local collagen disruption or proteoglycan concentrations as such covariates would presumably be closely related to cellular response. However, our model is presently trained to identify clones independent of surrounding tissue appearance, and as such it cannot provide any mechanistic or associative information relating chondrocyte proliferation to tissue structure/composition.

Secondly, the inter-observer agreement on clone identification using this definition was relatively lower (ICC = 0.76) than expert agreement achieved for identification of individual chondrocytes (ICC = 0.87).[25] However, given the much smaller number of clones in an image compared to the total number of chondrocytes, this reduction in ICC value is a function of disagreement on a very small number of clones in the full data set. Another limitation was that the YOLO detected some false positive clones among sparsely distributed chondrocytes and some false detections of small clone sizes (Figure 4). A possible reason for the false positives is that the training images included mostly clustered chondrocytes, leaving the model without sufficient training to recognize sparser chondrocyte patterns. A possible reason for identifying artificially small clones was that the YOLO was trained using rabbit cartilage and clones from rabbit cartilage are smaller than those that can develop in much thicker pig cartilage. Retraining using additional images of sparse chondrocytes, larger clones, and multiple species could potentially further improve performance over the good agreement with experts that was achieved with this version of the YOLO. Finally, there were few statistically significant differences in clone density associated with time after fracture in the minipig model of PTOA, which is attributed both to the presence of some clones in normal minipig talar cartilage, and to the small number of animals available for each study group (n = 5) in this secondary analysis of existing histological sections. As hypothesized, progressive chondrocyte/clone density changes were identified, although adequately powered future studies will be needed to fully document the natural history of chondrocyte activity in joints sustaining intra-articular fractures.

In conclusion, two CNN models were developed, validated, and implemented to document progressive changes in chondrocyte density & cloning in a minipig model of intra-articular fracture, which is known develop post-traumatic OA. The accuracy of the resulting chondrocyte segmentation and clone identification was very similar to the gold-standard of human expert chondrocyte/clone identification. This fully objectively obtained cellularity data could be incorporated into an automated image-analysis based histological scoring system for OA progression, or used as a stand-alone technique to quantify changes in cellularity and chondrocyte organization in articular cartilage. This deep-learning-powered approach provides objective and accurate cartilage health information and can thus better facilitate studies of cartilage injury and regeneration.

ACKNOWLEDGEMENTS

We would like to thank Dr Stephen Baek from Department of Industrial Engineering at the University of Iowa for providing expertise knowledge and suggestions in deep learning model development and training. Department of Defense grants W81XWH-10-1-0864, W81XWH-15-1-0642, and W81XWH-11-1-0583 provided funding for the original minipig studies from which the histological sections analyzed in this work were taken. NIH/NIAMS grant P50 AR055533 and Centers for Disease Control grant R49 CCR721745 funded the rabbit study which yielded the histology sections that underwent secondary analysis in this work. The content is solely the responsibility of the authors and the sponsor did not have any role in study design, data interpretation, or in the writing of

the manuscript. Opinions, interpretations, conclusions and recommendations are those of the author and are not necessarily endorsed by the U.S. Army. In conducting research using animals, the investigators adhere to the laws of the United States and regulations of the Department of Agriculture.

REFERENCES

1. Mankin HJ. Biochemical and metabolic aspects of osteoarthritis. The Orthopedic clinics of North America. 1971;2:19–31. [PubMed: 4940528]
2. Pritzker KPH, Gay S, Jimenez SA, et al. Osteoarthritis cartilage histopathology: grading and staging. Osteoarthritis and Cartilage. 2006;14:13–29. [PubMed: 16242352]
3. Pauli C, Whiteside R, Heras FL, et al. Comparison of cartilage histopathology assessment systems on human knee joints at all stages of osteoarthritis development. Osteoarthritis Cartilage. 2012;20:476–485. [PubMed: 22353747]
4. Moussavi-Harami SF, Pedersen DR, Martin JA, Hillis SL, Brown TDJJoOR. Automated objective scoring of histologically apparent cartilage degeneration using a custom image analysis program. 2009;27:522–528.
5. Pedersen DR, Goetz JE, Kurriger GL, Martin JA. Comparative digital cartilage histology for human and common osteoarthritis models. Orthopedic research and reviews. 2013;2013:13. [PubMed: 24465137]
6. Krizhevsky A, Sutskever I, Hinton GE. Imagenet classification with deep convolutional neural networks. Advances in neural information processing systems2012:1097–1105.
7. Ren S, He K, Girshick R, Sun J. Faster r-cnn: Towards real-time object detection with region proposal networks. Advances in neural information processing systems2015:91–99.
8. Redmon J, Divvala S, Girshick R, Farhadi A. You only look once: Unified, real-time object detection. Proceedings of the IEEE conference on computer vision and pattern recognition2016:779–788.
9. Ronneberger O, Fischer P, Brox T. U-net: Convolutional networks for biomedical image segmentation. International Conference on Medical image computing and computer-assisted intervention: Springer; 2015:234–241.
10. Girshick R. Fast r-cnn. Proceedings of the IEEE international conference on computer vision2015:1440–1448.
11. Tiulpin A, Klein S, Bierma-Zeinstra S, et al. Deep learning predicts knee osteoarthritis progression from plain radiographs. Osteoarthritis and Cartilage. 2019;27:S397–S398.
12. von Schacky CE, Sohn J, Foreman SC, et al. Development and performance comparison with radiologists of a multitask deep learning model for severity grading of hip osteoarthritis features on radiographs. Osteoarthritis and Cartilage. 2020;28:S306–S308.
13. Perslev M, Pai A, Igel C, Runhaar J, Dam EB. Validation of an open source, generic deep learning architecture for 3D MRI segmentation - with data from the OAI, PROOF, and CCBR. Osteoarthritis and Cartilage. 2019;27:S393–S394.
14. Tibrewala R, Pedoia V, Kinnunen C, Popovic T, Souza R, Majumdar S. Deep learning-based automatic estimation of volume and fat fraction in abductor muscles and their associations with T1RHO and T2 in hip osteoarthritis patients. Osteoarthritis and Cartilage. 2019;27:S384–S385.
15. Tibrewala R, Ozhinsky E, Shah R, Foreman SC, Pedoia V, Majumdar S. Detecting hip osteoarthritic degenerative changes in MRI using deep learning. Osteoarthritis and Cartilage. 2019;27:S387–S388.
16. Bejnordi BE, Veta M, Van Diest PJ, et al. Diagnostic assessment of deep learning algorithms for detection of lymph node metastases in women with breast cancer. Jama. 2017;318:2199–2210. [PubMed: 29234806]
17. Nagpal K, Foote D, Liu Y, et al. Development and validation of a deep learning algorithm for improving Gleason scoring of prostate cancer. NPJ digital medicine. 2019;2:1–10. [PubMed: 31304351]
18. Sornapudi S, Stanley RJ, Stoecker WV, et al. Deep learning nuclei detection in digitized histology images by superpixels. Journal of pathology informatics. 2018;9.

19. Wang H, Roa AC, Basavanhally AN, et al. Mitosis detection in breast cancer pathology images by combining handcrafted and convolutional neural network features. Journal of Medical Imaging. 2014;1:034003.
20. Sirinukunwattana K, Pluim JP, Chen H, et al. Gland segmentation in colon histology images: The glas challenge contest. Medical image analysis. 2017;35:489–502. [PubMed: 27614792]
21. Chen H, Qi X, Yu L, Dou Q, Qin J, Heng PA. DCAN: Deep contour-aware networks for object instance segmentation from histology images. Medical image analysis. 2017;36:135–146. [PubMed: 27898306]
22. Power L, Acevedo L, Yamashita R, Rubin D, Martin I, Barbero A. Deep learning enables the automation of grading histological tissue engineered cartilage images for quality control standardization. Osteoarthritis and Cartilage. 2021;29:433–443. [PubMed: 33422705]
23. Rutgers M, Van Pelt M, Dhert W, Creemers LB, Saris D. Evaluation of histological scoring systems for tissue-engineered, repaired and osteoarthritic cartilage. Osteoarthritis and cartilage. 2010;18:12–23. [PubMed: 19747584]
24. Rytky S, Huang L, Tiulpin A, et al. Deep learning-based segmentation from histology allows for automated quantification of calcified cartilage morphology in a rabbit model of post-traumatic osteoarthritis. Osteoarthritis and Cartilage. 2020;28:S310–S311.
25. Yang L, Coleman MC, Hines MR, Kluz PN, Brouillette MJ, Goetz JE. Deep Learning for Chondrocyte Identification in Automated Histological Analysis of Articular Cartilage. The Iowa Orthopaedic Journal. 2019;39:1.
26. Ioffe S, Szegedy CJapa. Batch normalization: Accelerating deep network training by reducing internal covariate shift. 2015.
27. Goodfellow I, Bengio Y, Courville A, Bengio Y. Deep learning: MIT press Cambridge; 2016.
28. Tochigi Y, Vaseenon T, Heiner AD, et al. Instability dependency of osteoarthritis development in a rabbit model of graded anterior cruciate ligament transection. The Journal of bone and joint surgery. American volume. 2011;93:640–647. [PubMed: 21471417]
29. Goetz JE, Coleman MC, Fredericks DC, et al. Time-dependent loss of mitochondrial function precedes progressive histologic cartilage degeneration in a rabbit meniscal destabilization model. Journal of orthopaedic research : official publication of the Orthopaedic Research Society. 2017;35:590–599. [PubMed: 27279147]
30. Van der Walt S, Schönberger JL, Nunez-Iglesias J, et al. scikit-image: image processing in Python. PeerJ. 2014;2:e453.
31. Goetz JE, Fredericks D, Petersen E, et al. A clinically realistic large animal model of intra-articular fracture that progresses to post-traumatic osteoarthritis. Osteoarthritis and Cartilage. 2015;23:1797–1805. [PubMed: 26033166]
32. Coleman MC, Goetz JE, Brouillette MJ, et al. Targeting mitochondrial responses to intra-articular fracture to prevent posttraumatic osteoarthritis. Sci Transl Med. 2018;10.
33. Rothe R, Guillaumin M, Van Gool L. Non-maximum suppression for object detection by passing messages between windows. Asian conference on computer vision: Springer; 2014:290–306.
34. Cowton J, Kyriazakis I, Bacardit J. Automated Individual Pig Localisation, Tracking and Behaviour Metric Extraction Using Deep Learning. IEEE Access. 2019;7:108049–108060.
35. Koo TK, Li MY. A Guideline of Selecting and Reporting Intraclass Correlation Coefficients for Reliability Research. Journal of chiropractic medicine. 2016;15:155–163. [PubMed: 27330520]
36. Girshick R, Donahue J, Darrell T, Malik J. Rich feature hierarchies for accurate object detection and semantic segmentation. Proceedings of the IEEE conference on computer vision and pattern recognition2014:580–587.
37. Kamisan N, Naveen SV, Ahmad RE, Kamarul T. Chondrocyte density, proteoglycan content and gene expressions from native cartilage are species specific and not dependent on cartilage thickness: a comparative analysis between rat, rabbit and goat. BMC Vet Res. 2013;9:62–62. [PubMed: 23547659]

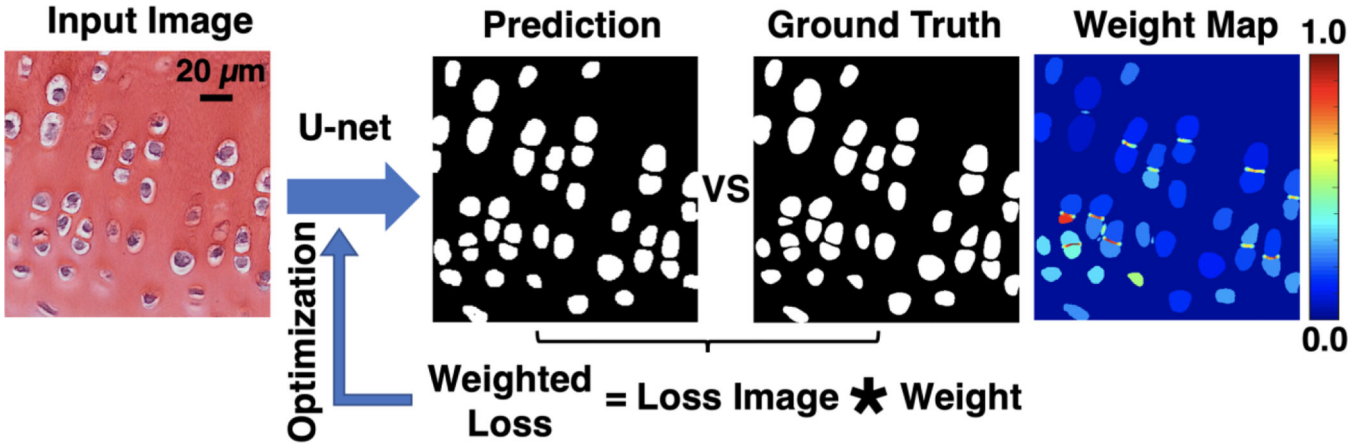

Figure 1:

This figure illustrates the U-Net model to developed to identify individual chondrocytes. The U-Net was trained to predict the segmentation image given an input histological section (top left). The difference between the predicted and ground truth segmentation image at each pixel is quantified using the binary cross entropy loss function and weighted using the pre-computed weight map (top right). Pixels of smaller cells in the ground truth segmentation image were assigned higher weight values (warmer color), forcing the U-Net to identify smaller chondrocytes. Pixels between closely adjacent chondrocytes (distance less than 1.5 microns) in the ground truth segmentation image are also assigned with higher weight value, which forced the U-Net to learn to separate adjacent chondrocytes.

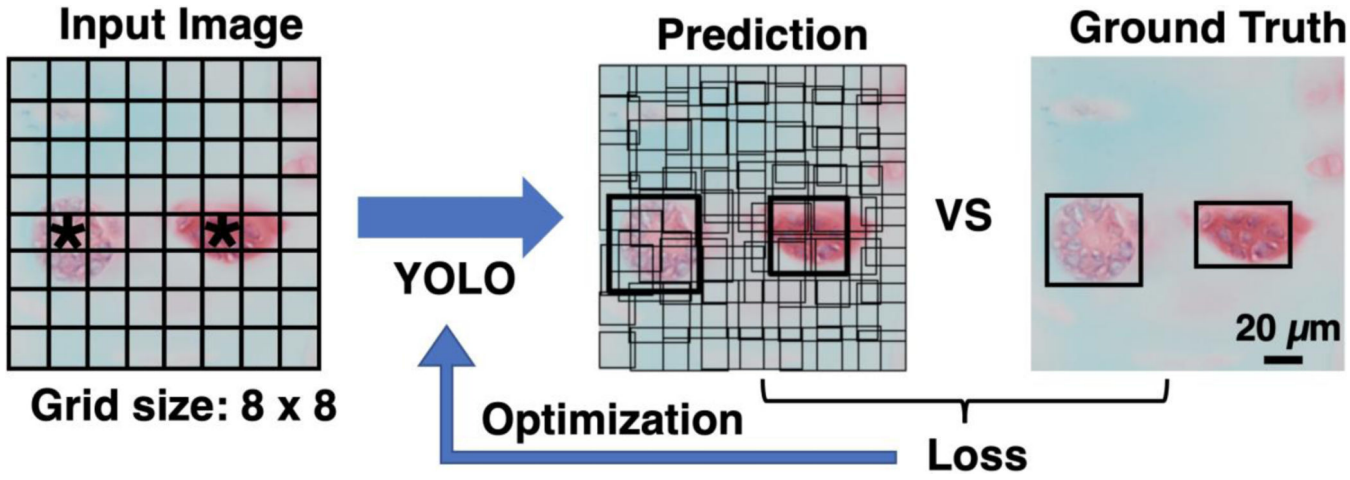

Figure 2:

This figure illustrates the YOLO model developed to identify chondrocyte clones. The YOLO implementation predicted a total of 64 bounding boxes, one at each cell of an 8×8 grid spanning the entire input image. This allowed the detection of multiple clones in a single image. If the center of an annotated clone lies within a grid cell, only the associated bounding box (e.g., two thicker boxes in the prediction) in that grid cell should be predicted by the model to match the coordinates of the ground truth box of that clone, and the predicted probability value should approach 1; if a grid cell does not contain a clone's center, the associated box from that grid cell should be simply predicted with a probability value of 0, and its coordinates do not matter. In practice, the probability value is a continuous number ranging between 0 and 1 and a predicted bounding box with probability value larger than 0.5 is considered a clone.

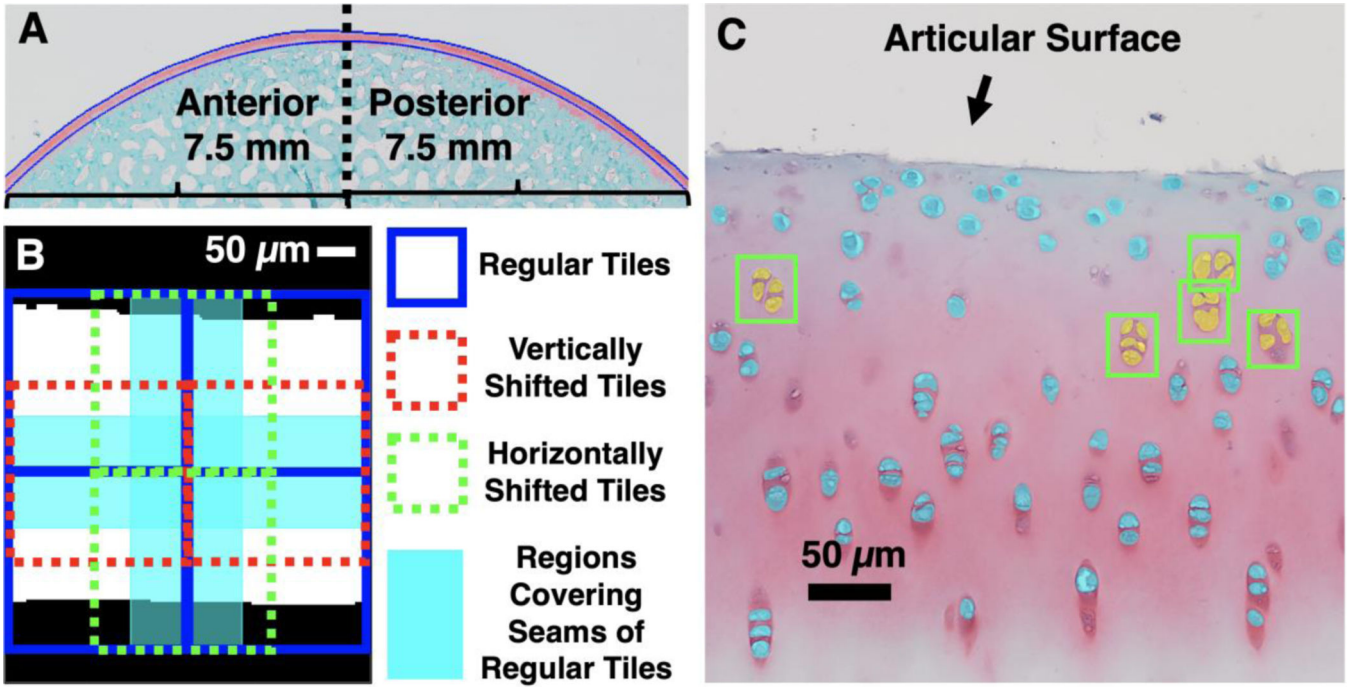

Figure 3:

This figure illustrates the method to analyze the weightbearing area of the minipig talus cartilage. A) For a given digitized histological section, the center of the weight bearing area was determined (vertical dash line), and 15-mm horizontal span of cartilage (7.5 mm for both the anterior and posterior) was segmented (blue boundaries) to be analyzed. B) Illustration of the sliding window approach to cover the segmented cartilage in an example cartilage segmentation (white region). A window slides from top to bottom in a column-by-column-basis with the stride of the window side length to cover the whole segmented cartilage. These regular windows are offset by half of window side length in vertical and horizontal direction to cover the seams between regular windows. Image tiles are cropped from all the window locations and analyzed by the U-net and YOLO models. C) Resulting cell segmentations and clone detections on cartilage by the U-net and YOLO projected back to the cartilage. Individual chondrocytes segmentations from the U-net were compared to the clones (green bounding boxes) detected by the YOLO in order to divide chondrocytes into clone chondrocytes (yellow segmentations) and regular chondrocytes (cyan segmentations).

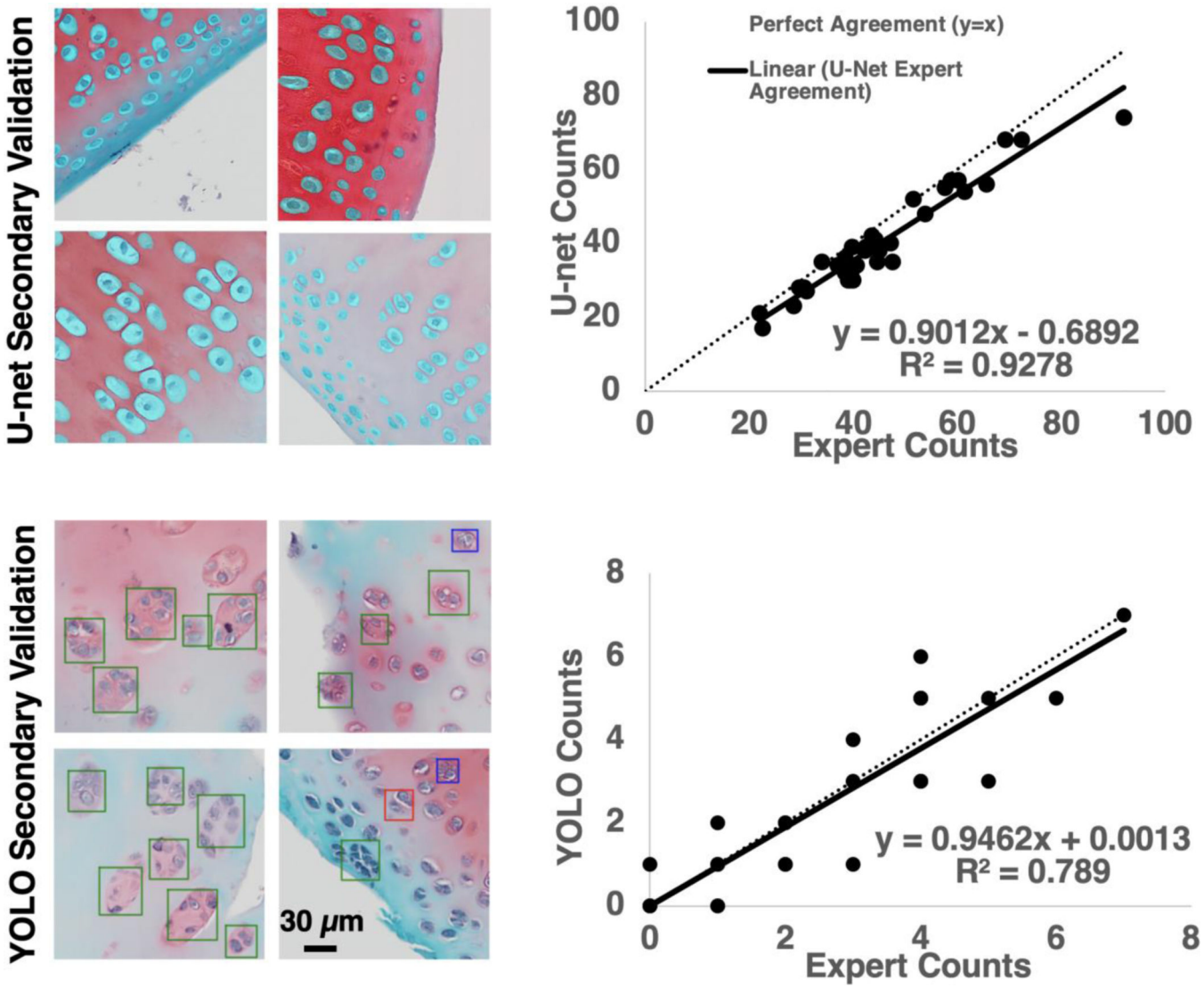

Figure 4:

(Upper) The trained U-net was able to accurately detect chondrocyte of different size, shape, appearance and zonal origin. It has achieved an excellent agreement with expert researchers on counting chondrocytes. (Lower) The trained YOLO model was able to accurately detect clones of different sizes and geometry, with few false positive (red box) or false negative (blue boxes). The trained YOLO model achieved good agreement with expert researchers on identifying clones on 30 images not used to train the model.

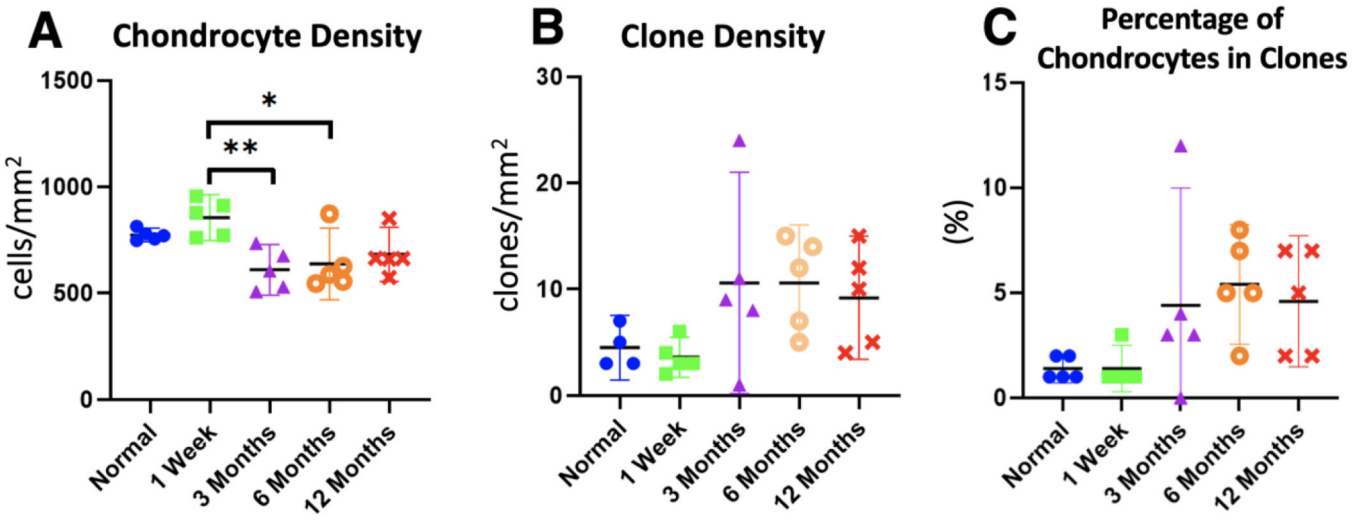

Figure 5:

This figure shows the plots of chondrocytes density, clone density, and percentage of chondrocytes in clones at different post-operative timepoints from the entire cartilage region. A) Chondrocyte densities in the entire cartilage span demonstrated a slight increase one week after fracture and then decreased after 3 months. The asterisk (*) indicates level of significance: * for $p < 0.05$ and ** for $p < 0.01$. B, C) Clone densities/percentages of chondrocyte in clone were low in the normal and early (one week) after fracture and increased after 3 months, although this increase was not significant.

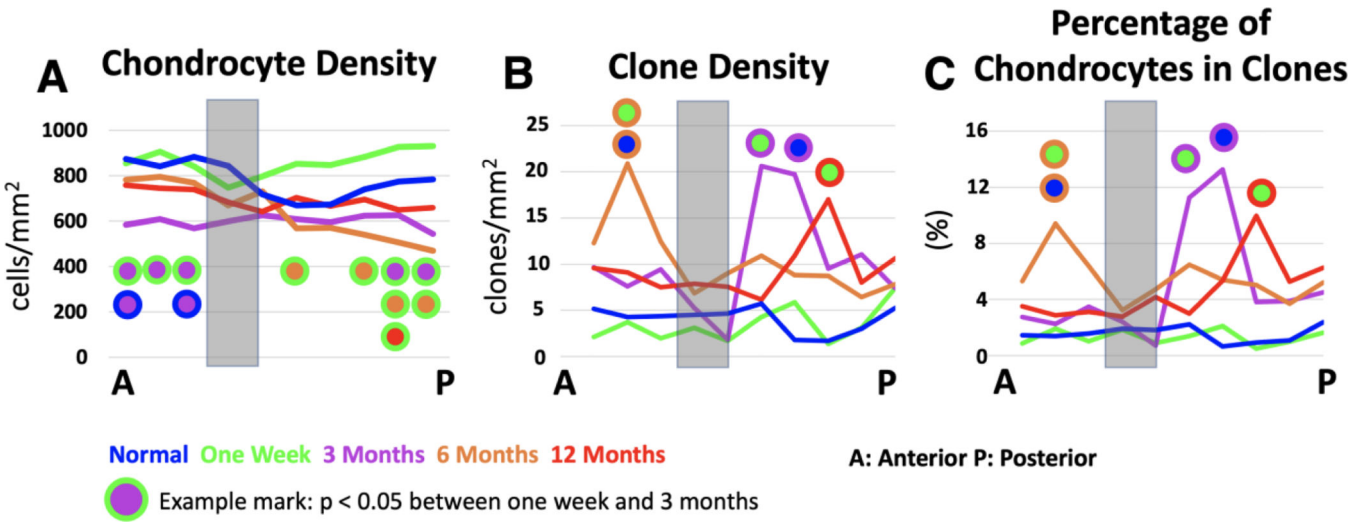

Figure 6:

Maps of chondrocyte density, clone density, and percentage of chondrocytes in clones plotted in 1.5 mm increments along the weightbearing cartilage surface. The gray bar indicates the part of the talus in direct contact with the fracture line during the fracture-inducing impact. The curve for each timepoint represents the mean cellularity metric value among the 5 different animals at that timepoint. Color-filled circles represent pair-wise comparisons with $p < 0.05$. A) Chondrocyte densities in normal and one-week post-fracture tissue were higher than at later post-fracture time points, particularly the 3-month time point and along the anterior portion of the weightbearing cartilage. B, C) Significantly higher values of clone density and the percentage of chondrocytes in clones were found 3, 6, and 12 months after fracture. Compared to the relative uniformity of clone distribution over the weightbearing cartilage in the normal and 1-week post-fracture groups, the local increases in clone density adjacent to the tissue damaged by the fracture indicate the pathological nature of the clones detected by our model.

Table 1:

This table summarizes chondrocyte density values (cells/mm^2) at different post-operative timepoints. Values are mapped in 10% increments across the weightbearing articular cartilage surface and shown as a mean with lower and upper 95% confidence interval bounds. The articular surface between 30% to 40% (shaded columns) was the portion of the talus that articulated with the fracture line in the tibia.

		Anterior					Posterior					Entire Surface
		10%	20%	30%	40%	50%	60%	70%	80%	90%	100%	
Normal	Mean	868	848	903	814	708	701	673	729	719	730	774
	Lower	1035	987	1149	914	797	886	789	798	824	876	742
	Upper	701	709	656	715	618	517	557	660	615	584	806
One Week	Mean	899	903	846	795	810	837	816	864	923	918	856
	Lower	1027	979	942	936	966	997	933	959	1015	977	748
	Upper	772	826	750	654	654	678	698	768	830	859	963
3 Months	Mean	583	609	568	600	626	609	595	625	627	545	610
	Lower	661	694	715	716	772	891	822	823	807	958	491
	Upper	506	524	421	483	479	327	368	426	447	131	729
6 Months	Mean	782	795	769	669	731	568	572	540	505	470	638
	Lower	862	975	1135	947	1151	730	774	776	701	818	470
	Upper	701	615	402	391	311	405	369	304	310	121	806
12 Months	Mean	759	745	739	685	643	704	668	696	650	660	683
	Lower	1048	991	888	821	803	1122	861	832	815	818	556
	Upper	470	498	590	548	483	285	475	560	486	502	810

Table 2:

This table summarizes clone density (clone count), with values expressed as clones/mm^2 (number clones) at different post-operative timepoints. Values are mapped in 10% increments across the weightbearing articular cartilage surface and shown as a mean with lower and upper 95% confidence interval bounds. The articular surface between 30% to 40% (shaded columns) was the portion of the talus that articulated with the fracture line in the tibia.

		Anterior					Posterior					Entire Surface
		10%	20%	30%	40%	50%	60%	70%	80%	90%	100%	
Normal	Mean	5 (2)	4 (1)	4 (2)	4 (2)	5 (2)	6 (2)	2 (1)	2 (1)	3 (1)	5 (2)	5 (14)
	Lower	0 (0)	0 (0)	0 (0)	0 (0)	0 (0)	0 (0)	0 (0)	0 (0)	0 (0)	2 (1)	1 (5)
	Upper	12 (4)	12 (3)	10 (5)	15 (7)	11 (4)	15 (5)	5 (2)	5 (2)	6 (3)	8 (3)	8 (23)
One Week	Mean	2 (1)	4 (1)	2 (1)	3 (1)	2 (1)	4 (1)	6 (2)	1 (0)	3 (1)	7 (3)	4 (11)
	Lower	0 (0)	0 (0)	0 (0)	0 (0)	0 (0)	0 (0)	0 (0)	0 (0)	0 (0)	0 (0)	2 (4)
	Upper	8 (3)	12 (4)	8 (2)	10 (3)	5 (2)	7 (3)	14 (3)	4 (1)	9 (3)	16 (6)	5 (19)
3 Months	Mean	10(6)	8(5)	9(5)	5(3)	2(1)	21(9)	20(12)	10(5)	11(6)	8(5)	11(58)
	Lower	0(0)	0(0)	0(0)	0(0)	0(0)	0(0)	0(0)	0(0)	0(0)	0(0)	0 (3)
	Upper	21 (12)	21 (13)	20 (11)	18 (11)	6 (3)	44 (19)	51 (30)	21 (11)	27 (14)	18 (10)	21 (113)
6 Months	Mean	12 (7)	21 (12)	13 (7)	7 (5)	9 (6)	11 (7)	9 (5)	9 (6)	6 (5)	8 (7)	11 (68)
	Lower	0(0)	0(0)	0(0)	0(0)	0(0)	2(3)	2(2)	0(0)	0(0)	0(0)	5 (44)
	Upper	31 (17)	42 (26)	28 (18)	18 (13)	20 (15)	19 (11)	16 (9)	18 (12)	17 (14)	18 (15)	16 (92)
12 Months	Mean	9 (4)	9 (3)	8 (3)	8 (4)	7 (4)	6 (4)	11 (7)	17 (13)	8 (5)	11 (8)	9 (58)
	Lower	0 (0)	0 (0)	2 (1)	0 (0)	3 (3)	2 (0)	0 (0)	0 (0)	2 (1)	1 (0)	3 (12)
	Upper	18 (7)	21 (4)	13 (8)	16 (5)	11 (8)	11 (8)	22 (16)	36 (29)	14 (9)	20 (17)	15 (98)